Chapter 4

Geology, Textural Study, Ore Genesis and Processing of the Tabuaço Tungsten Deposit (Northern Portugal)

Yann Foucaud, Bénédicte Lechenard,
Philippe Marion, Inna Filippova and Lev Filippov

Additional information is available at the end of the chapter

http://dx.doi.org/10.5772/intechopen.71674

Abstract

The Tabuaço tungsten deposit (Northern Portugal) is hosted in the Cambrian Douro Group metasediments, at the northern margin of the Beira-Tabuaço granitic complex. The hosting schisto-calcareous Lower Cambrian Bateiras Formation underwent a contact metamorphism induced by the intrusion of the granitic complex. The skarnification led to the crystallisation of scheelite ($CaWO_4$). Two different skarn facies are encountered: 'Lower Skarn' and 'Main Skarn' both corresponding to the exoskarn. The 'Main Skarn' is mainly composed of vesuvianite ($Ca_{10}Mg_2Al_4(SiO_4)_5(Si_2O_7)_2(OH)_4$), feldspars and fluorite. Zoisite, grossular, fluorapatite and scheelite are also present, as well as malayaite and cassiterite. Scheelite is disseminated and often occurs in association with fluorite, albite and vesuvianite. The 'Lower Skarn' level contains predominantly diopsidic pyroxene, quartz, zoisite, grossular and feldspars. Scheelite appears both laminated and disseminated, in association with fluorite and vesuvianite in minor proportions. The 'Main Skarn' is located in the Garnet, Pyroxene zone, while the 'Lower Skarn' corresponds to the Pyroxene, Garnet zone. Pyroxene has a global hedenbergite Hd_{40} composition. A major phase of albitisation destabilised fluorite, scheelite, vesuvianite, garnet and pyroxene. A late stage of chloritisation is associated with the exhumation. The processing of the Tabuaço ore has been adapted to the Ca-bearing rich paragenesis and to the scheelite mean size.

Keywords: skarn, scheelite, texture, paragenesis, processing

1. Introduction

The European Union has classified tungsten in 2010 as a critical raw material (CRM) [1]. This decision is based not only on the very high economic importance of tungsten in the European

industry but also on the high supply risk to the member countries [2]. Indeed, in 2010, among the 16 world tungsten producers, China supplied 86% of the 72,100 tons of the global production [3].

This current situation results from the precipitous fall of tungsten price caused by Chinese dumping of low-operating-cost tungsten into global markets in the 1980s (**Figure 1**) [4]. Price remained low until 2005, preventing from any mining investment in other countries. Since then, China imposes quotas on its tungsten exports to preserve its own industry as a result of the growing worldwide domestic demand [3]. As a consequence, tungsten price has increased considerably for the last two decades, stimulating a gradual upturn of the exploration (**Figure 1**).

Tungsten is extracted from wolframite ((Fe, Mn, Mg)WO_4) and scheelite ($CaWO_4$). These two minerals can be found in Sn-W quartz veins, often associated with the Variscan orogenic cycle [5]. However, the major occurrence of scheelite is in skarn-type and skarnoid-type ores, related to a thermo-metamorphism of carbonated rocks. Historically, tungsten ores were predominantly processed by gravity techniques, often combined with magnetic separation, as W-bearing mineral density contrasts with gangue minerals [6]. Over the past decades, the explored tungsten ores have exhibited more and more fine-grained and in close association with gangue minerals, leading to the development of flotation as the main beneficiation route [7–9]. Nowadays, tungsten concentrates, assaying 20 to 65% WO_3, are mostly processed by hydrometallurgy and impurities such as phosphorus, silica and fluorine must be removed as much as possible in the preceding steps [10–12]. Mineral processing stage is consequently crucial in the elimination of the contaminant-bearing gangue minerals prior to hydrometallurgy. During beneficiation, W-bearing minerals are separated from the gangue minerals by physical processes, such as gravity and magnetic separation, and by physico-chemical processes as flotation. Performance of such separations requires a thorough knowledge of

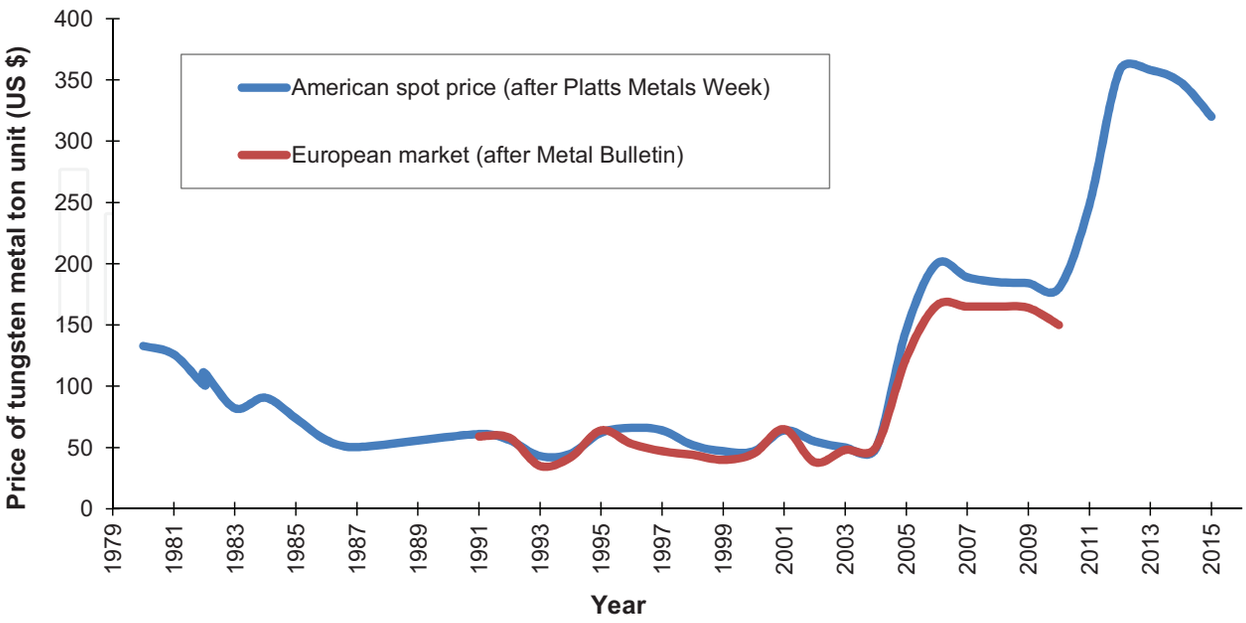

Figure 1. Evolution of tungsten metal ton unit price over the past decades.

http://dx.doi.org/10.5772/intechopen.71674

the ore mineralogy including mineralogical and textural characterisation. Thus, the adoption of a systemic geometallurgical approach integrating studies from exploration to metallurgy ensures the best recovery of the valuable tungsten metal. This chapter presents mineralogical and textural studies performed on the Tabuaço tungsten skarn ore as a basis of the ore metallogeny. Results are used to design the optimum ore separation process.

2. Regional geology

2.1. Centro-Iberica zone

The Tabuaço deposit is located in the Central Iberian Zone (CIZ), one of the six zones composing the Iberian Massif (**Figure 2**), which is the part of the Variscan Belt in the Iberian Peninsula

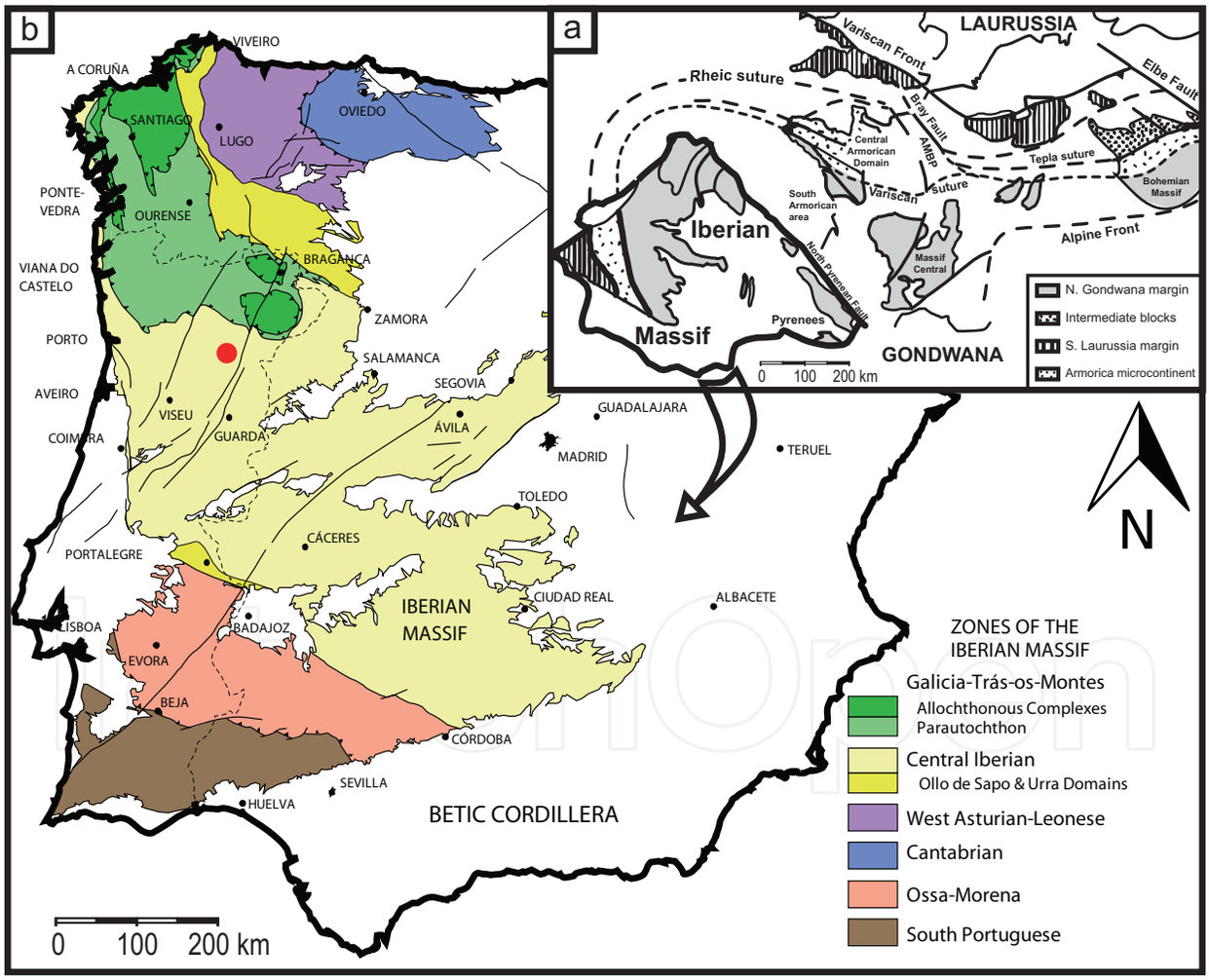

Figure 2. (a) Simplified tectonic sketch of the West European Variscan Belt showing the main occurrences of high-pressure rocks, modified after Faure et al. [13]. (b) Map showing the outcrops of the Variscan basement in the Iberian Peninsula and the zones of the Iberian Massif, modified after Martínez Catalán [14]. Red circle shows the location of the deposit.

[14, 15]. Details of the geodynamic evolution of the Variscan Belt have been extensively described [16–18]. The closing of the Iapetus and Rheic oceans during the Silurian-Devonian induced a collision between the two supracontinents Gondwana and Laurussia. The different zones were sutured to form a vast chain, covering all the Western Europe (**Figure 2**), called the Variscan Belt. The majority of the inner part of this chain, including the studied area, underwent a polyphased tectono-metamorphic evolution, going through at least three deformation stages and a regional green schist metamorphism [14].

2.2. Sedimentary formations

The Bateiras Formation is part of the Douro Group metasediments which are included in the Dúrico-Beirão Supergroup, also named 'Schist-Greywacke Complex' (SGC). The Douro Group is characterised by metapelitic rocks interlayered by metagraywacke and calcsilicate rocks [19]. The Bateiras Formation is constituted by a succession of metagraywackes/metaconglomerates and black schists at the basis and by a succession of graphite-bearing black schists, black schists and calcareous layers [20, 21] going towards the youngest direction. The layers are centimetric to metric, for a global thickness of 800 ± 100 m [19]. This formation can be attributed to a terrigenous sedimentation at the basis, changing gradually to a basin sedimentation, occurred between 565 and 550 Ma [22, 23]. The whole Dúrico-Beirão Supergroup has then undergone the Variscan regional deformation and metamorphism described before.

2.3. Granitic intrusives

The intrusion of the Paredes da Beira-Tabuaço granite (PBT) leads to the formation of the Tabuaço W-skarn. The batholith extends over 200 km^2 and is zoned by three different medium-grained facies, known as Paredes da Beira-Tabuaço granite (outer zone), Sendim-Laboreira granite (middle zone) and Aricera granite (inner zone) [21, 24]. Some aplitic and pegmatitic bodies, closely associated with the granite, were reported by previous authors [25], associated with the crystallisation of the last magmatic liquids. The Paredes da Beira-Tabuaço granite stricto sensu contains quartz, two feldspars (Na-feldspar and K-feldspar), two micas (muscovite and biotite) and apatite [25]. The mineralogical association suggests that the granite is peraluminous as confirmed by a 1.08 < A/CNK < 1.32 [25]. Low contents of MgO (≤ 0.06%), CaO (≤ 0.6%) and $(Fe_2O_3)_{tot}$ (≤ 1%) were reported for the PBT granite [25]. The PBT granite is part of Tabuaço granite massif, considered as tardi-D3 [25, 26], and yields K-Ar biotite and muscovite ages of 310 Ma [26]. Most recently, Rb-Sr. system is used on bulk on aplitic and pegmatitic bodies as well as on the Tabuaço granite yields with age of 311 ± 7 Ma [25, 27]. The Sr. and Nd isotopic compositions prove that these S-type granites are set up from a parental magma generated by the anataxis of the Grupo do Douro metasediments [25, 27].

3. Deposit geology

The Tabuaço tungsten deposit is located at the northern margin of the PBT granite and hosted in metamorphic rocks from the Bateiras Formation (**Figure 3**). It consists of two

http://dx.doi.org/10.5772/intechopen.71674

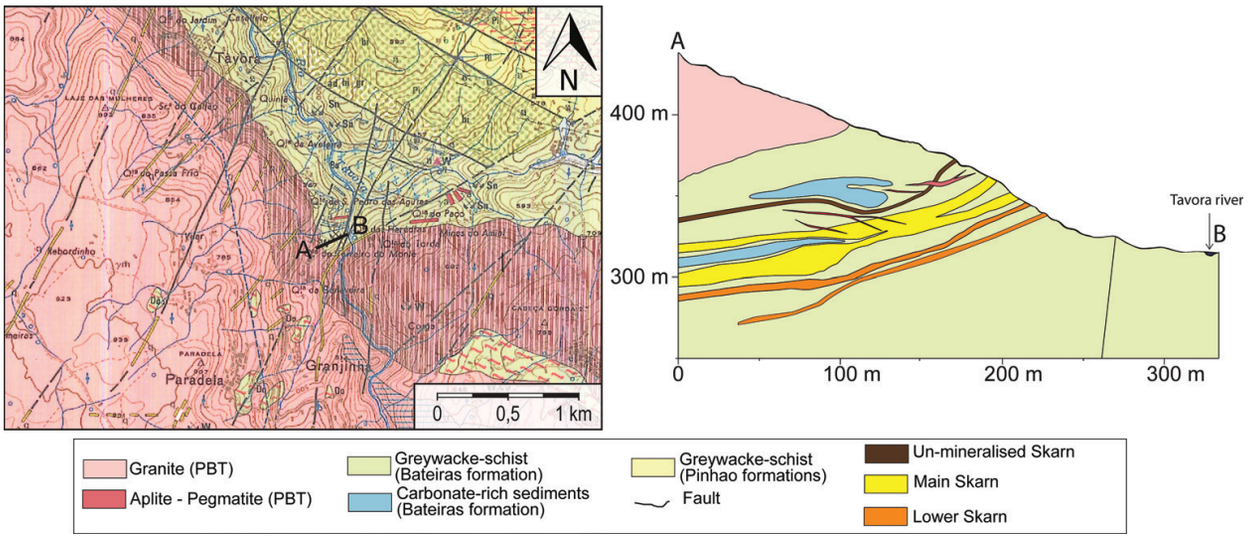

Figure 3. Left: Geological map of the studied area showing the Paredes da Beira-Tabuaço (PBT) granitic intrusion and the hosting Bateiras sedimentary formation (source: LNEG). Right: NE-SW cross section along the A-B line, based on Colt Resources drilling data and showing the main geological units of the Tabuaço deposit.

subdeposits referred as Aveleira and São Pedro das Águias. The study focusses on the latter, which represents 71% of the whole Tabuaço deposit. São Pedro das Águias deposit is composed of around 100 m of sedimentary rocks in which two mineralised units are included. Colt Resources reported in 2011 that a NI 43–101 indicated and inferred resource of 2 M.t. with a 0.56% WO_3 average grade, ranking Tabuaço as a middle-sized world-class tungsten deposit [28]. The two mineralised units, called 'Lower Skarn' and 'Main Skarn', are subparallel to the contact between the PBT granite and the Bateiras Formation, with a global strike-dip of N140–20°SW (**Figure 3**). The two horizons are completely different in terms of mineralogical association (presence/absence of pyroxene, abundance of garnet, etc.) and tungsten average grade (0.3% WO_3 for the Lower Skarn, 1% WO_3 for the Main Skarn), which can be related to their distance to the granite intrusion. The PBT granite intrusion occurred during the third tectono-metamorphic stage of the Variscan Belt, during which the global strike of shear zones, faults and fold axis was NW-SE [14]. Hence, the granite intrusion and the related skarn-hosted Tabuaço mineralisation are controlled by these structural deformations (**Figure 3**).

4. Sampling and analytical methods

Diamond drill programmes were performed by Colt Resources. Cores were used to characterise the deposit geology in terms of textures and mineralogy. Based on these analyses, a sampling campaign has been organised, and 330 kg of each of the two outcropping mineralised layers were sampled. On both the drill cores and the samples, thin polished sections were realised, scanned and analysed with, firstly, an optical microscope and then with a scanning electron microscope (SEM) Hitachi S-4800. This SEM utilises an electron beam accelerated from 500 V to 30 kV. The acceleration voltage used there was 15 kV.

Local chemical analyses on minerals were performed using a CAMECA SX100 Castaing electron microprobe. The acceleration voltage used there was 15 kV. Each analysis lasted 3 min and permitted to measure the composition of 15 elements in all the studied minerals, with a lateral resolution lower than 1 μm. Based on the results, structural formula of each mineral was then reconstituted.

Chemical analyses were carried out by inductively coupled plasma-mass spectrometer (ICP-MS) for the trace elements and by inductively coupled plasma-optical emission spectrometer (ICP-OES) for the major elements. Fluorine was analysed by direct ionometry and CO_2 by IR spectroscopy after combustion, with a C-S analyser. All these analyses were performed on representative pulverised samples at the Service d'Analyse des Roches et des Minéraux (SARM-CNRS, Nancy, France).

5. Results

5.1. Geochemistry of the mineralised layers

Geochemical analyses show that the two skarn units are significantly different in terms of chemistry, which partly explains the variety of mineral paragenesis (**Table 1**). The SiO_2 content within the calcareous rocks controlled the mineralogical assemblage resulting from the metasomatism event: silicates (including quartz) are predominant in the Lower Skarn, while the Main Skarn is enriched in calcium-bearing silicates and calcium-semi-soluble salts. In addition, the Lower Skarn has a higher Fe_2O_3 content and a lower CaO content than the Main Skarn (**Table 1**). Such differences in the chemistry between the skarn horizons must relate to the variation in chemistry of the protoliths since the PBT granite is too poor in Fe or Ca to induce such enrichments.

Notable W grade variation exists between the two skarn horizons (**Table 1**), the Main Skarn being more than eight times richer compared to the Lower Skarn. The differences in protolith chemistry and distance from the granite intrusion are two main controls of the W grade. As the Main Skarn is more proximal to the granite than the Lower Skarn

	SiO_2 (%)	Al_2O_3 (%)	Fe_2O_3 (%)	MgO (%)	CaO (%)	Na_2O (%)	K_2O (%)	P_2O_5 (%)	F (%)	CO_2 (%)	As (ppm)	W (%)	LOI (%)	Tot (%)
Main Skarn	37.81	17.45	2.39	1.66	31.56	1.32	0.72	0.73	5.6	0.18	18.8	1.7	5.09	98.98
Lower Skarn	47.25	17.14	6.06	2.31	21.38	1.86	0.94	0.33	1.47	0.16	180.7	0.23	2.17	100.16

Table 1. Chemical analyses showing major elements, some trace elements, F and CO_2 contents of the two mineralised layers.

http://dx.doi.org/10.5772/intechopen.71674

(**Figure 3**), and presents higher CaO content, fluids were W-richer and scheelite precipitated preferentially.

Arsenic distribution within the skarns is also spatially zoned (**Table 1**). Very low grades are recorded in the Main Skarn, ten times lower than the ones in the Lower Skarn. Arsenic likely origins are from magmatic fluids associated with the granite intrusion, and mineralisation occurs in the vicinity or at the immediate proximity of a reduced layer.

5.2. Macroscopic scale study

The 'Main Skarn' unit presents massive, coarse-grained textures, strongly overprinting the almost lost sedimentary features during the metamorphism events (**Figure 4a**, **b** and **d**). Average grain size ranges between few micrometres to more than 1 cm. Some rock samples show weakly banded local features, which can be interpreted as a relic of the varying chemical composition between the layers of the Bateiras Formation or as a late albite vein-controlled deposition (**Figure 4b** and **c**).

In terms of mineralogy, sizeable amounts of honey-coloured fluorite are clearly visible macroscopically, associated with other minerals in pluri-millimetric patches (**Figure 4a**, **b**). In the samples, scheelite is easily identifiable under a short-wavelength UV-ray lamp, as it is a fluorescent mineral (**Figure 4**). Scheelite is mostly finely disseminated, forming micrometre- to centimetre-scaled crystal aggregates (**Figure 4a**, **b** and **d**). These aggregates are probably composed of an association between scheelite and other minerals, the accurate spotting of scheelite being difficult with UV-ray lamp due to the diffusion of the fluorescence light.

The 'Lower Skarn', located in the distal part of the skarn deposit, shows quite well-preserved sedimentary features. Macroscopic banded textures (**Figure 4e–h**) are interpreted as a result of the bimetasomatism phenomenon, developed between centimetric sedimentary layers with varying chemical compositions. The preservation of the initial macroscopic structure is directly linked to the temperature gradient from the intrusion heat source and then the degree of the bimetasomatism. This latter has been nearly complete in the Main Skarn but only partial in the Lower Skarn. However, it has been powerful enough to permit the formation of calcic silicates in all the layers (**Figure 4e** and **h**).

In the Lower Skarn, macroscopic identification is much more difficult because of the very fine-grained texture. However, centimetric patches of vesuvianite, a common Ca-bearing hydrated silicate in skarns, are visible associated with pinkish K-feldspars and green pyroxene (**Figure 4g**). Even if zoisite, a calcic epidote-group mineral, is stable in all the mineralogical association, some light-green layers are notably enriched (**Figure 4e**). As well, pyroxene-rich and vesuvianite-rich zones are alternating in some samples (**Figure 4f** and **h**). Green zones contain pluri-millimetric sulphide crystals, being mainly arsenopyrite and pyrrhotite (**Figure 4d** and **f**). Such zones are rare in the skarns and represent some reduced levels, with high sulphur content, weakly affected by the metasomatic and metamorphic processes. An

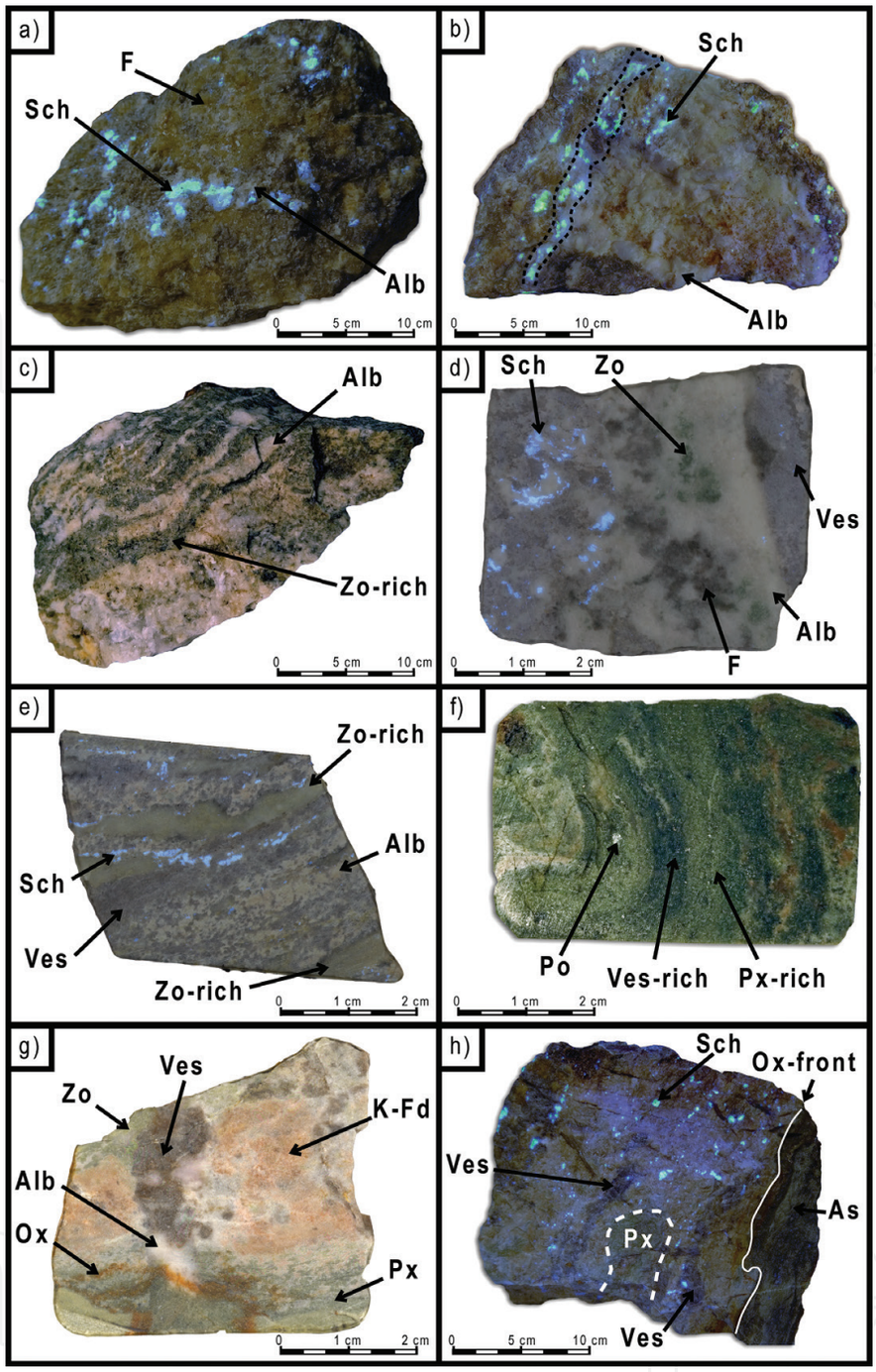

Figure 4. Photographs of hand samples showing major mineralogical assemblages and textures of the Main Skarn (a to d) and the Lower Skarn (e to h) under natural light associated with a short-wavelength UV-ray lamp. (a) Disseminated scheelite with large patch of honey-coloured fluorite. (b) Laminated scheelite close to albite and fluorite. (c) Banded texture showing alternating zoisite-rich zones and albite veins. (d) Penetrative texture of albite into vesuvianite + scheelite + fluorite assembly. (e) Inherited banded texture with laminated scheelite along the sedimentary layer boundaries. (f) Sulphide-rich green zone presenting a succession of vesuvianite-rich and pyroxene-rich zones. (g) Progressive change from a pyroxene-rich zone to a K-feldspar + vesuvianite zone, associated with albite. (h) Scheelite occurring both as disseminated and laminated and associated with a pyroxene-rich zone and vesuvianite patches. Note the oxidisation front, separating the sulphide-rich zone (right) from the sulphide-depleted zone (left). Sch, scheelite; Ves, vesuvianite; Zo, zoisite; F, fluorite; Alb, albite; As, arsenopyrite; Po, pyrrhotite; Ox, oxides; Px, pyroxene; K-Fd, K-feldspars.

http://dx.doi.org/10.5772/intechopen.71674

oxidation front clearly separates reduced sulphide-rich zones and oxidised sulphide-depleted zones (**Figure 4h**). In the oxidised zone, vesuvianite is clearly identified macroscopically, forming large areas of dark prisms.

In terms of W mineralisation, in the Lower Skarn, poorer than the Main Skarn, only rare occurrences of disseminated scheelite can be observed macroscopically (**Figure 4h**). Noteworthy, the two mineralised skarns (Lower and Main) also present laminated scheelite which seems controlled by the chemical composition of the hosting sedimentary layers (**Figure 4b** and **e**).

Albite is largely present in the two mineralised horizons, occurring in veins (**Figure 4b** and **c**) or associated with other minerals such as vesuvianite (**Figure 4g** and **d**). It seems that albite veins are penetrative into the skarns. A correlation exists macroscopically between the presence of albite and the absence of scheelite (**Figure 4d** and **e**).

5.3. Visible light and electron microscope scale study

Thin sections were observed under optical microscope and under scanning electron microscope. While scheelite appears laminated in hand samples, microscopically, all the observed scheelite is finely disseminated and forms anhedral crystals with sizes of between 5 and 300 μm for the Main Skarn (**Figure 5a** and **b**) and below 150 μm for the Lower Skarn. These values are considered as the liberation mesh required for an efficient ore separation process.

Molybdenum content was measured in the scheelite using the Castaing electron microprobe. Regardless of the Skarn horizon type, very low grades were found, 0 to 0.12% MoO_3 with an average of 0.029% MoO_3. The scheelite is zoned, with grain cores richer in MoO_3 than the rims.

Scheelite grains are closely associated with vesuvianite (**Figure 5a**; **Figure 7a**), which forms large areas, above all in the Main Skarn (**Figure 5a**), as the main calcium-bearing silicates of the global mineralogical association (Main and Lower Skarns). Structural formula shows no variation between the Lower Skarn and the Main Skarn, being $(Ca_{9.36}Mg_{0.41})(Al_{1.13}Fe_{0.80}Mg_{0.07})Al_4[(Si_{8.83}Al_{0.09})O_{32.39}F_{1.61}]$ with traces of strontium, manganese and phosphorus. Hence, fluorovesuvianite is stable in the whole skarn body, regardless of the temperature or the chemistry of the protoliths.

Close association between vesuvianite and euhedral garnets (**Figure 5c**) proves their synchronous formation. Besides, the fact that their chemical analyses are similar indicates that temperature rather than fluid chemical properties controls the precipitation of one mineral over the other one. Microprobe analyses give an average structural formula of $(Ca_{2.99}Sr_{0.01})(Al_{1.75}Fe_{0.25})[(Si_{2.87}Al_{0.1})O_{11.6}F_{0.4}]$ for all the analysed garnets, which are individually represented in a ternary diagram (**Figure 6**, left). Analysed garnets are from the Main Skarn horizon only, as very few garnets are present in the Lower Skarn. In summary, garnets are $Gr_{87}And_{13}$, proving the predominance of Al^{3+} and Ca^{2+} on Fe^{3+} and Fe^{2+}, respectively.

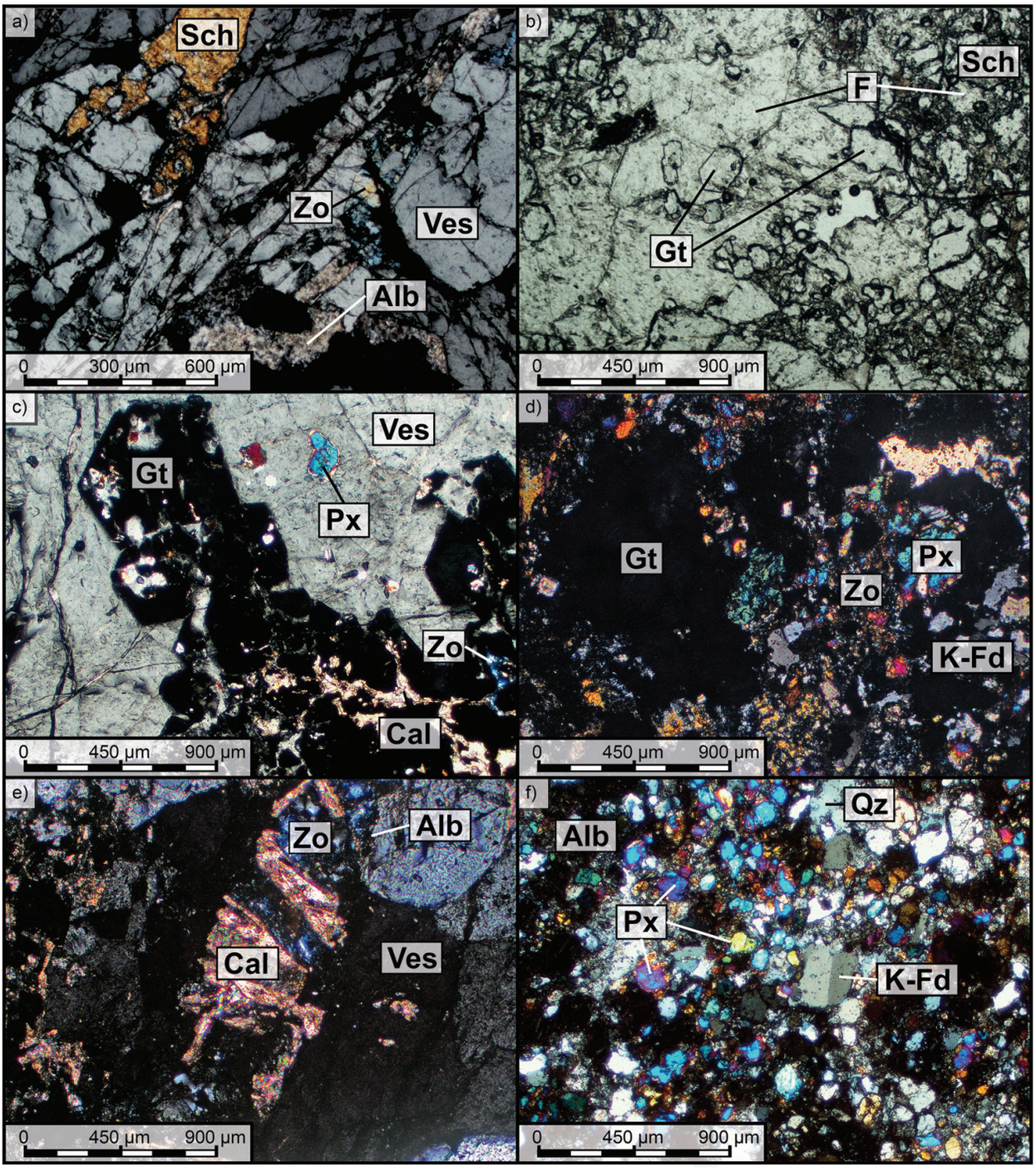

Figure 5. Photographs of thin sections observed with optical microscope in cross polarised light (a, c to f) and in polarised light (b) showing different microscopic textures and mineral assemblage in the Main Skarn (a to c) and in the Lower Skarn (d to f). (a) Vesuvianite area containing both scheelite and zoisite with a kaolinised albite alteration. (b) A typical association between scheelite, garnet and fluorite. (c) Synchronous formation of euhedral garnets and vesuvianite, containing a clinopyroxene, with a tardive setup of calcite + epidote. (d) Poikilitic texture of coexisting clinopyroxene and garnet, finely associated with K-feldspars and zoisite. (e) Vesuvianite crystal altered into albite with calcite + epidote overprint. (f) Typical mineral association of the Lower Skarn, composed of pyroxene, feldspars, zoisite and minor quartz. Same legend as **Figure 4** with Qz, quartz; Cal, calcite; Gt, garnet.

Very rare crystals of clinopyroxene are present in the Main Skarn level, often included in vesuvianite grains (**Figure 5c**). In the Lower Skarn, clinopyroxene is predominant over garnet. However, some poikilitic textures of garnets surrounding pyroxene are found (**Figure 5d**),

http://dx.doi.org/10.5772/intechopen.71674

proving the coexistence of both in the Lower Skarn, where the pyroxene is closely associated with quartz, K-feldspars and zoisite (**Figure 5f**). The centimetric layers observed macroscopically have been described as alternating pyroxene-rich levels, inducing the green colour, and quartz/K-feldspars/vesuvianite-rich levels (**Figure 4f**, **g** and **h**). Optical factors indicate that the pyroxene has an intermediate composition between hedenbergite (Fe) and diopside (Mg) poles of calcic clinopyroxene continuous series. This observation is confirmed by electron microprobe analyses, which permitted to calculate a global average formula of $Ca_{1.01}(Fe_{0.40}Mg_{0.59}Mn_{0.01})[(Si_{1.98}Al_{0.01})O_6]$ for the Lower Skarn, as no pyroxene of the Main Skarn could be analysed. The pyroxene is then $Hd_{40}Di_{59}Jo_1$.

Zoisite, clearly identified microscopically (**Figure 5a**, **c**, **d** and **e**; **Figure 7c** and **e**), is frequently zoned, probably admitting significant variations in the chemistry. Electron microprobe showed that zoisite has a significant part of the aluminium substituted by Fe^{2+} and Mg^{2+} (in smaller proportions) in the octahedral sites. The calculated structural formula, $Ca_{2.02}(Al_{2.59}Fe_{0.37}Mg_{0.01})[(Si_{2.99}Al_{0.01})O_{10.38}(OH)_{0.62}]$, indicates that it is a Fe-rich zoisite, called after Fe-zoisite. The Fe-zoisite is present in both Main and Lower Skarns and seems stable in the mineralogical association. Sizeable amounts of Fe-zoisite are associated with calcite in micro-veins (**Figure 5e**), postponing the albite previously described. These veins are cross-cutting the whole samples, visible macroscopically on the thin sections.

Another major mineral of the paragenesis is fluorite, which forms centimetric patches, often in association with vesuvianite and scheelite in the Main Skarn (**Figure 5b**; **Figure 7a**, **b** and **e**). Fluorite is also closely associated with pyroxene in the Lower Skarn while less abundant. Microprobe analysis shows that vesuvianite and apatite bear fluorine, in substitution of the hydroxyl group. They are then fluoro-vesuvianite and fluorapatite, respectively. Garnet also bears fluorine, in substitution of oxygen.

A late albitisation stage is responsible for the destabilisation of the metasomatism-related mineral association. This alteration is promoted by cross-cutting micro-veins of albite (**Figure 5a** and **e**; **Figure 7b**). Most of the albite is developed at the selvedge of the grains

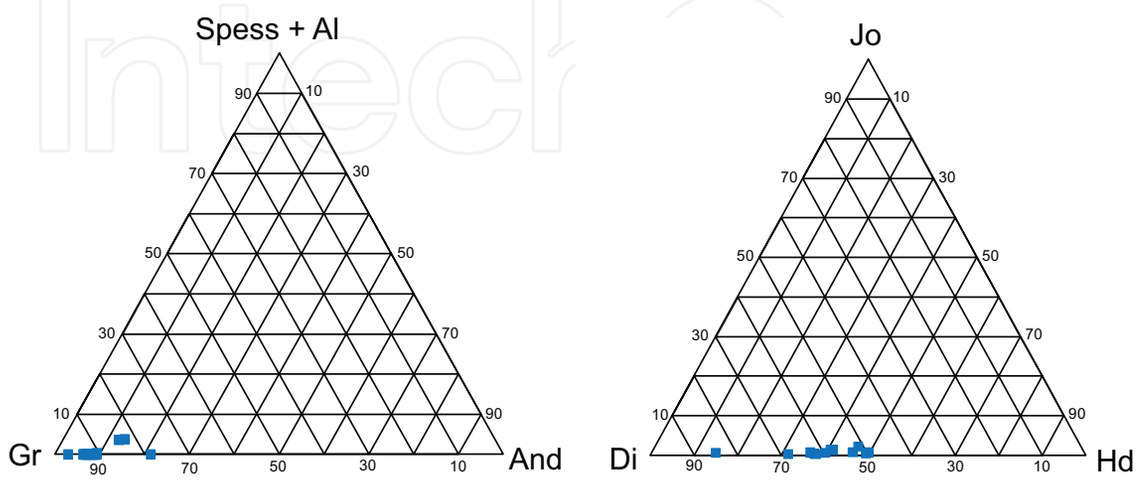

Figure 6. Ternary diagram showing composition of garnets from the Main Skarn, between andradite (And), grossular (Gr) and spessartine + almandine (Spess + Al) (left), and composition of clinopyroxene from the Lower Skarn, between hedenbergite (Hd), diopside (Di) and Johannsenite (Jo) (right).

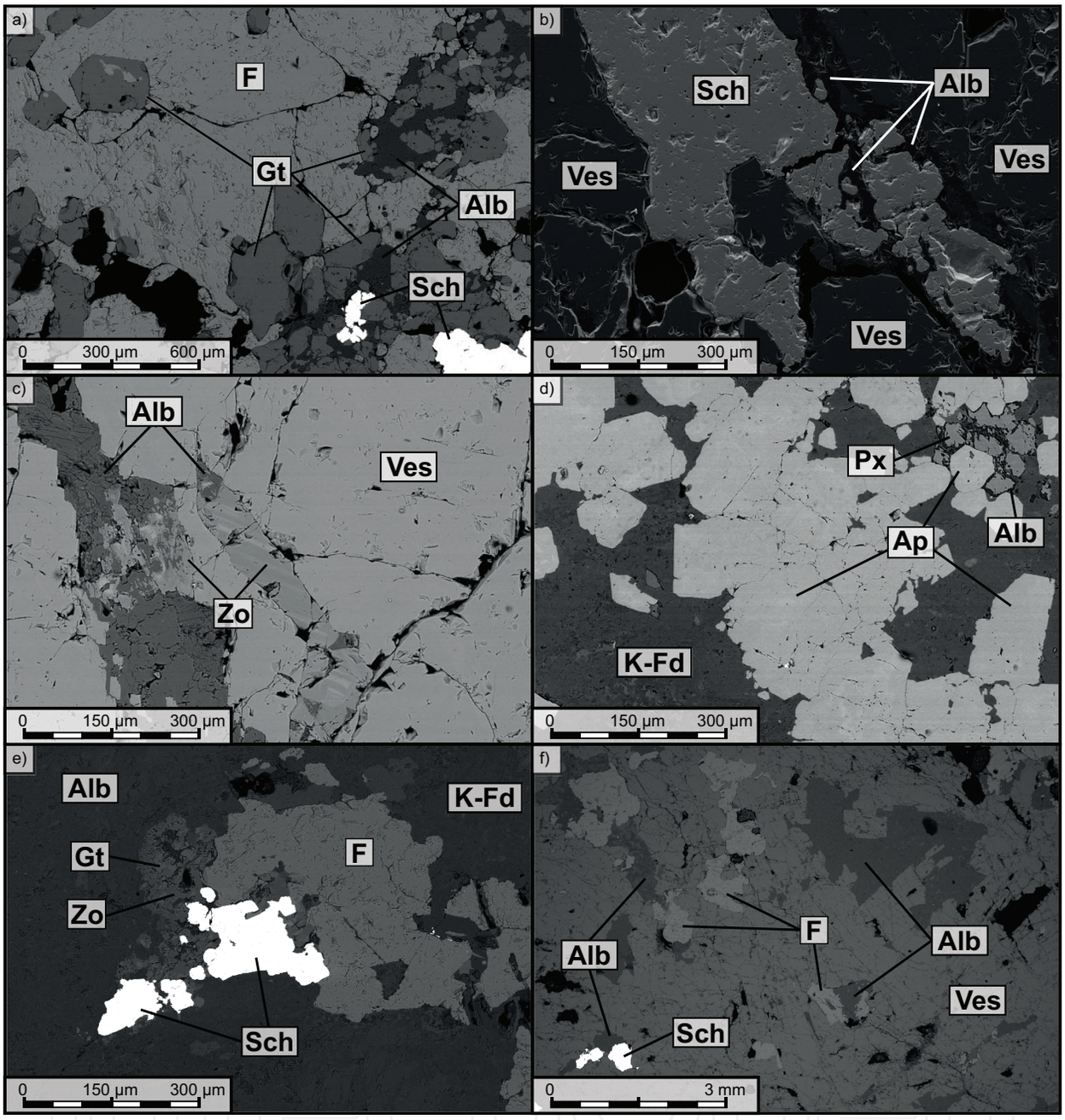

Figure 7. SEM images of Main Skarn thin sections, in back-scattered electrons imaging (a, c to f) and in secondary electron imaging (b), showing different textures on the ore. (a) Association of scheelite, garnet, fluorite and vesuvianite, the garnet being unsettled by albite. (b) Association of scheelite and vesuvianite, with an albite micro-vein unsettling vesuvianite at the grain joint. (c) Zonation in a zoisite, which is being unsettled by albite. (d) Apatite with K-feldspars and pyroxene, being consumed by albite. (e) Close association between scheelite, fluorite, garnet and zoisite, surrounded by albite. (f) Scheelite and fluorite being unsettled by albite. (Same legend as **Figures 4** and **5**).

(**Figure 7c** and **d**). The shape of the original crystal is preserved, forming phantoms of primary minerals (**Figure 7a**, **c** and **f**). Destabilisation textures, such as very fine intergrowth of albite along the 90° cleavages of fluorite at the beginning which generalises after (**Figure 7f**),

http://dx.doi.org/10.5772/intechopen.71674

can be observed for most of the minerals: garnet (**Figure 7a**), vesuvianite (**Figure 7b** and **f**), zoisite and even scheelite (**Figure 7f**).

6. Discussion

6.1. General discussion

Microprobe analyses indicate that scheelite is zoned in terms of Mo-content. This phenomenon is explained by the low sulphur content in the hosting sedimentary rocks, as no molybdenite was found. Molybdenum, in very low amount, originates from magmatic fluids and is incorporated into the scheelite crystals, contributing to the continuous solid solution between scheelite ($CaWO_4$) and powellite ($CaMoO_4$). The low content of molybdenum in scheelite suggests a high quality of this W deposit, as molybdenum represents a critical penalising element for tungsten metal properties. Some authors reported that Mo-poor scheelite is associated with oxidised skarns [29]. More recent studies proved that Mo-poor scheelite can as well form in reduced skarns [30–32]. Based on the later classifications [31], the Tabuaço skarn is a reduced skarn. Indeed, it presents Mo-poor scheelite which is related to a low dioxygen fugacity [30], high pyrrhotite:pyrite ratios and grossular-rich garnet (Gr_{87}). The andradite content is very low in the garnet, for which the Al^{3+}/Fe^{3+} ratio is around 7.4. Moreover, all the other Fe-bearing minerals are all Fe^{2+}-bearing minerals (vesuvianite, pyroxene and epidote). All these elements are suggesting that fluids going from the granitic intrusion to the hosting sedimentary rocks are reduced, with low dioxygen fugacity and then low Fe^{3+}/Fe^{2+} ratio.

Scheelite crystallisation is controlled by pH and Ca^{2+} activity in the hosting rocks, as the tungsten is transported by acidic magmatic fluids in the form of tungstic acid [30]. A brutal increase of the pH or of the Ca^{2+} concentration in the fluids, as it would happen when cross-cutting a carbonate-rich horizon, can lead to the precipitation of scheelite [30, 33]. Hence, laminated scheelite would have primary precipitated at the contact of carbonate-rich layers of the sediment. A fluid grade of 100 ppm of W is reported to be enough to cause scheelite precipitation at the vicinity of a carbonated layer [33]. Disseminated scheelite, sparser, likely results from a remobilisation of the laminated scheelite, postponing bimetasomatism reactions which led to the loss of the initial heterogeneity of the sedimentary hosting rocks.

The two mineralised horizons correspond to carbonate-rich layers alternating with thin levels of silicate-rich sediments. This succession allowed the crystallisation of calcium-bearing silicates by a bimodal exchange between the two categories of sediments (bimetasomatism). However, the Lower Skarn protolith was probably more silicate-rich than the Main Skarn protolith. The dominance of calcium in Main Skarn induced the formation of sizeable amounts of semi-soluble salts, as scheelite, fluorite and apatite. These two latter crystallised as a result of an increase of Ca^{2+} and even more importantly F^- and PO_4^{3-} activities in the fluids. These volatile-enriched fluids correspond to end-magmatic crystallisation fluids and explain the substitution of hydroxyl group or of oxygen by fluorine in apatite, vesuvianite

and garnet [30, 32]. The fluorine origin is probably sedimentary, as the granite is a peraluminous S-type granite, formed by anatexis of the Bateiras Formation. Some Mo-poor W-F skarns, derived from S-type granite intrusions, were described by authors [34]. The composition of fluids is generally intermediate between oxidised and reduced, and the skarn cannot be really classified [32].

Tin-bearing minerals are also present in minor amounts. It consists of cassiterite and malayaite, two calcium/tin-bearing silicates which presence has been several times reported by authors in a similar context [29, 30, 35].

Furthermore, the mineralisation is closely linked to the setup of the skarn induced by the intrusion of a S-type peraluminous tardi-D_3 of two mica granites (PBT granite). In the late stage of crystallisation, fractionated fluids were enriched in some elements (W, F, P). Their slow diffusion into the hosting rocks, from the granite to the metamorphosed sediments, was driven mainly by the temperature gradient and variations in chemical potential [30, 36]. As the hosting sediments were composed of silicate-rich and carbonate-rich centimetric to metric layers, very associated, each brutal change induced a rebalancing of the fluids with the rock (**Figure 9**). Scheelite, fluorite and apatite precipitated when both the Ca^{2+} activity and the pH increased suddenly, at the contact with the carbonated layers (**Figure 9**). Because of its proximal location to the granite, the temperature is higher in the Main Skarn than in the Lower Skarn, inducing a faster and nearly complete homogenisation of the initial banded textures. Difference in temperature also explains the dominance of the garnet in the Main Skarn and the dominance of the pyroxene in the Lower Skarn, consolidated by chemical contrast. Indeed, the crystallisation of pyroxene requires more SiO_2 compared to the garnet, and bulk analyses showed that the Lower Skarn is SiO_2-richer (**Table 1**). In addition, the graphite content seems

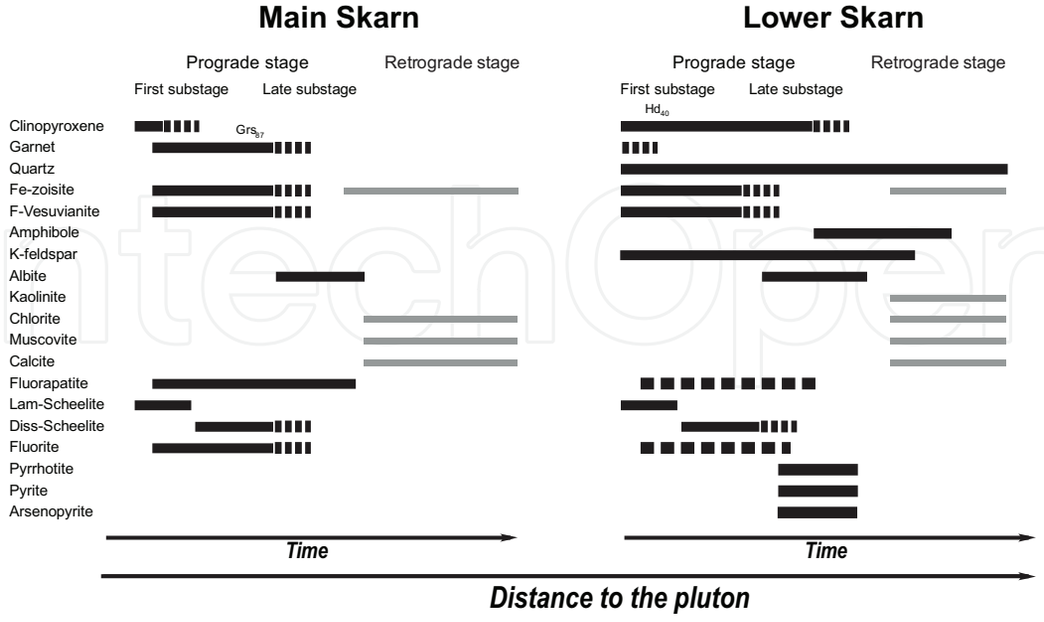

Figure 8. Paragenetic sequence of the Tabuaço scheelite skarn, showing the evolution of the mineral associations versus time and versus distance to the pluton (i.e. for the two skarn horizons).

http://dx.doi.org/10.5772/intechopen.71674

to play a role in the variation of skarn composition [30, 37] as a graphite-rich layer will lead to the formation of Pyr > Gar and pyrrhotite > > pyrite zone as observed in the Lower Skarn. Finally, the Tabuaço skarn is spatially zoned (**Figure 9**) with a Gar > Pyr zone transitioning to a Pyr < Gar zone. The latter zone contains sizeable amounts of sulphides, mainly pyrrhotite and arsenopyrite, which reflects the high sulphur and probably graphite content of the hosting sediments (**Figure 9**). It could correspond to the graphite-bearing shales, occurring in the Bateiras Formation.

The skarn zonation has been intensively described by authors [30, 32, 35, 38] and could be summarised as follows, from the pluton to the metamorphic marbles: **Quartz ± Garnet (inferred) → Garnet > Pyroxene (Main Skarn) → Pyroxene > Garnet (Lower Skarn) → Pyrrhotite zone → Wollastonite ± Quartz ± Calcite (inferred) → metamorphic marbles (Figure 9)**.

No evidence of wollastonite was found in the mineralogical observations. The presence of high content in aluminium, due not only to the peraluminous nature of the granite but also to the chemistry of the sediments, induced the formation of aluminium-bearing calc-silicates as vesuvianite, garnet and epidote, more favourably than the formation of wollastonite. But,

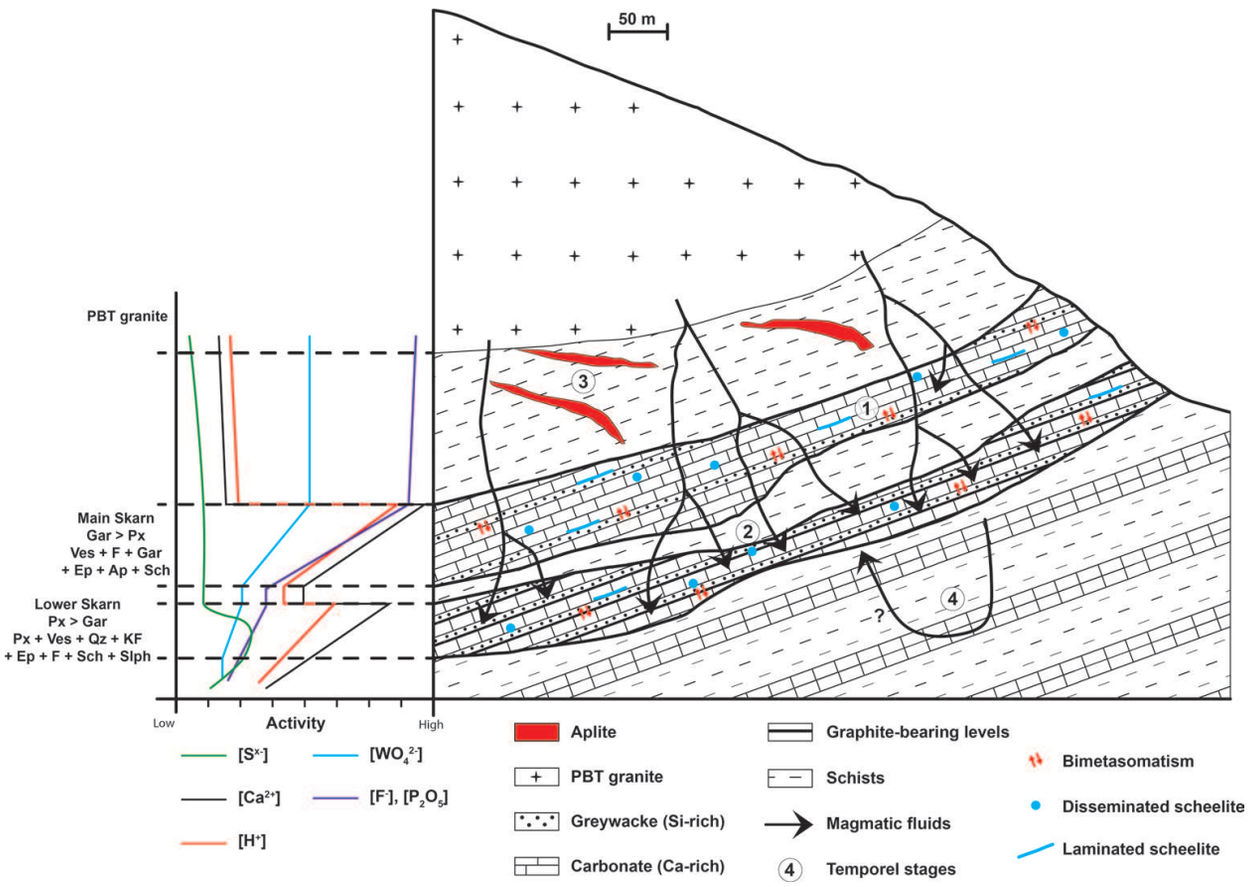

Figure 9. Schematic cross section of the Tabuaço deposit showing the spatial zonation and the temporal stages of mineral association. (See the text for further explanations.) Gar, Garnet; Px, pyroxene; Ves, vesuvianite; F, fluorite; Ep, epidote; Ap, apatite; Sch, scheelite; Qz, quartz; KF, K-feldspars; Slph, sulphides.

distal to the pyrrhotite-rich zone, described by the authors [30, 35], a wollastonite-rich zone could exist, even if it may be absent in several world skarns [39].

Within this zonation, vesuvianite is present and stable everywhere in the Gar > Pyr and in the Pyr > Gar zones, as well as zoisite (**Figure 9**). These two minerals are primary, based on the mineralogical observations, and associated with other primary minerals as fluorite, scheelite, apatite and garnet/pyroxene. Authors reported that zoisite can be primary, as a replacement of anorthite feldspar often described but absent in the Tabuaço mineral association [30]. As well, fluorite and apatite are stable in both the Main and Lower Skarns, their different contents being explained by the depletion of the F and P contents in the fluids reaching the distal part of the skarn (**Figure 9**). The same phenomenon occurred with the W content (**Figure 9**).

Authors reported that the formation of garnet and pyroxene occurs at least for 300°C [30, 40], while the zoisite epidote does not form under 445°C [32]. Pyroxene is probably formed first and unsettled in the skarn evolution by the garnet, as poikilitic textures are observed in this ore and have been observed for other ores [32]. Pyroxene is transformed into garnet when the fluids become SiO_2-richer and, above all, saturated [30, 41], occurring in the early prograde evolution.

The late prograde stage is characterised by the circulation of Na-rich fluids, which corresponds to the last fluids, enriched in incompatible elements by the fractionated crystallisation (**Figure 9**). These fluids come probably with the important intrusion of aplite veins at the immediate vicinity of the granite. Na-rich fluids started to unsettle the primary mineral association, transforming garnets, pyroxene, fluorite, vesuvianite and even scheelite into albite. However, this phenomenon is only partial in the skarn.

Finally, the retrograde stage is represented by an inverse fluid circulation, introduced few decades ago [29]. In the Tabuaço skarn, this late stage is characterised by an epidote + calcite association, mainly formed in the form of cross-cutting veins, postponing all the primary minerals. Some white micas (muscovite) and chlorite-group minerals have been observed, corresponding to the retrograde late stage. Supergene alteration induced the kaolinisation of the majority of albite formed in the skarn.

7. Conclusion: integrated mineralogy into a geometallurgical approach

A detailed mineralogical study of the skarn-hosted Tabuaço deposit was performed on rock sampled from two different skarn horizons. Mineralogical assemblages and textural observations are key elements to integrate into the beneficiation process design.

To begin with, consideration of the liberation mesh is primordial for the optimisation of the grinding steps. Liberation mesh was evaluated by optical microscopy under short-wavelength UV lamp and confirmed by geochemical analysis of the different size fraction. Liberation was estimated at an average size of 150 μm for both units, while it is recognised that the Lower Skarn unit has slightly smaller scheelite grains averaging around 120 μm.

http://dx.doi.org/10.5772/intechopen.71674

Then, the present study enabled to characterise mineralogical associations and crystallisation/alteration textures. In this regard, a feature of interest is the close association of the valuable scheelite with vesuvianite which is one of the major mineral phases. Metasomatism reactions led to the crystallisation of various calcium-bearing gangue silicates such as vesuvianite, garnet, pyroxene and epidote for the major ones. Thus, the main challenge in recovering scheelite versus calcium-bearing minerals via flotation processes is their selective separation due to the similarities in terms of surface properties, electrokinetics and stability/solubility in aqueous solutions. Conventional silicate depressants, for example, sodium silicate, exist, but the issue can only be resolved if the Ca^{2+} site-specific collector selectivity is high. Because of their different spatial relationship to the main granite intrusion along with the variation in protoliths lithology and chemical compositions, the two skarn horizons studied present distinct mineralogical assemblages. Thus, flotation reagents in terms of collector and depressant need to be tailored to the ore feed composition. No matter how successful the recovery of scheelite is, the concentrate grade can only be maximised if the grade of gangue minerals is reduced. For instance, fluorite is a major phase in the Main Skarn unit, and special effort should be taken to minimise its grade in the final concentrate.

Crystallisation textures are also essential to take into account in seeking and improving the concentrate grade. In particular, mineral intergrowth, poikilitic texture, micro-veins and secondary overprint are typical features of mixed particles occurring even if the liberation mesh is reached. Such mixed particles are likely to be harder to float, and in the eventuality that they are floated, the concentrate grade will be diluted by impurities.

Moreover, a pervasive albitisation of the skarn horizons, principally the Main Skarn, affects the whole prograde paragenesis, including scheelite. The overprint of albite onto scheelite grains inhibits the collector action, reducing significantly the concentrate grade and the overall recovery. In addition, albite has been subsequently altered into kaolinite and other clay minerals. These fragile minerals are concentrated in the very fine fractions (−10 μm) generated by the comminution steps; hence, it is crucial to perform a desliming step in order to remove this phase.

The optimisation of the flotation process should also consider the downstream treatments such as hydrometallurgy processes. In this regard, the concentration of penalising elements such as phosphorous should be limited. Fluorapatite, occurring predominantly in the Main Skarn horizon, requires the use of specific depressants to inhibit the action of Ca^{2+} site-specific collector. The Lower Skarn horizon is less challenging in terms of gangue mineral depression given the dominance of easily depressed silicates such as quartz, K-feldspar or pyroxene and the rare abundance of fluorapatite, fluorite or garnet.

Acknowledgements

The research leading to these results has received funding from the European Union's Horizon 2020 research and innovation programme under grant agreement No. 641650 for the

FAME project. This chapter reflects only the authors' view, exempting the commission from any liability. The authors would like to thank Gaëtan Fillon, Gabriel Crumiere and Frédéric Diot for their active collaboration in this work.

Author details

Yann Foucaud, Bénédicte Lechenard, Philippe Marion, Inna Filippova and Lev Filippov*

*Address all correspondence to: lev.filippov@univ-lorraine.fr

Université de Lorraine, GeoRessources, UMR 7359 UL-CNRS, Vandoeuvre-lès-Nancy, France

References

[1] European Commission. Critical Raw Materials for the EU: Report of the Ad-Hoc Working Group on Defining Critical Raw Materials. 2010. http://ec.europa.eu/enterprise/policies/rawmaterials/documents/index_en.htm

[2] Dewulf J, Blengini GA, Pennington D, Nuss P, Nassar NT. Criticality on the international scene: Quo vadis? Resources Policy. 2016;**50**(2016):169-176

[3] Audion AS, Labbé JF. avec la collaboration extérieure de la Compagnie Européenne d'Intelligence Stratégique (CEIS), 2012. Panorama mondial 2011 du marché du tungstène. Rapport Public. BRGM/RP-61341-FR, 108 p., 29 fig., 16 tabl. In French

[4] Lassner E, Schubert WD. Tungsten: Properties, Chemistry, Technology of the Element, Alloys and Chemical Compounds. 1999

[5] Jébrak M, Marcoux E. Geology of Mineral Resources. 2015

[6] Burt R. The role of gravity concentration in modern processing plants. Minerals Engineering. 1999;**12**(11):1291-1300

[7] Agar GE. Scheelite Flotation Process. Patent specification 4488959, USA, 17 p. 1982

[8] Atademir MR, Kitchener JA, Shergold HL. The surface chemistry and flotation of Scheelite. II. Flotation "collectors". International Journal of Mineral Processing. 1981;**8**:9-16

[9] Hiçyìlmaz C, Atalay Ü, Özbayoglu G. Technical note. Selective flotation of scheelite using amines. Minerals Engineering. 1993;**6**(3):313-320

[10] Pastor H. Métallurgie et Recyclage Du tungstène. 2000. Procédés. Dossier – Techniques de l'Ingénieur

[11] Yang Y, Xie B, Wang R, Xu S, Wang J, Xu Z. Extraction and separation of tungsten from acidic high-phosphorus solution. Hydrometallurgy. 2016;**164**(2016):97-102

[12] Zhang G, Guan W, Xiao L, Zhang Q. A novel process for tungsten hydrometallurgy based on direct solvent extraction in alkaline medium. Hydrometallurgy. 2016; **165**(2016):233-237

[13] Faure M, Cocherie A, Gaché J, Esnault C, Guerrot C, Rossi P, Wei L, Qiuli L. Middle carboniferous intracontinental subduction in the outer zone of the Variscan Belt (Montagne noire axial zone, French massif central): Multimethod geochronological approach of polyphase metamorphism. Geological Society, London, Special Publications. 2014;**2014**(405):239-311

[14] Martínez Catalán JR. The central Iberian arc, an orocline centered in the Iberian massif and some implications for the Variscan belt. International Journal of Earth Science (Geol Rundsch). 2012;**101**:1299-1314

[15] Julivert M, Fontboté J-M, Ribeiro A, Conde L. Mapa Tectónico de la Península Ibérica y Baleares E. 1:1,000,000. 1972. Inst. Geol. Min. España, Madrid

[16] Edel JB, Schulmann K, Skrzypek E, Cocherie A. Tectonic evolution of the European Variscan belt constrained by paleomagnetic, structural and anisotropy of magnetic susceptibility data from the northern Vosges magmatic arc (eastern France). Journal of the Geological Survey, London. 2015;**170**:785-804

[17] Faure M, Bé Mézème E, Cocherie A, Rossi P, Chemenda A, Boutelier D. Devonian geodynamic evolution of the Variscan Belt, insights from the French massif central and massif Armoricain. Tectonics. 2008;**27**:TC2005

[18] Tait JA, Bachtadse V, Franke W, Soffel HC. Geodynamic evolution of the European Variscan fold belt : Paleomagnetic and geological constraints. Geologische Rundschau. 1997;**86**:585-598

[19] Sousa MB. Litoestratigrafia e Estrutura Do «Complexo Xisto-Grauváquico» - Grupo Do Douro (Nordeste de Portugal). PhD thesis. University of Coimbra; 1982

[20] Dias R, Ribeiro A, Coke C, Pereira E, Rodrigues J, Castro P, Moreira N, Rebelo J. Evolução Estrutural Dos Setores Setentrionais Do Autoctone Da Zona Centro-Ibérica. 2013. Geologia de Portugal, vol. 1

[21] Pinto MD. Estudo comparativo de litologias calcosilicatadas e quartzo-pelíticas da Formação de Bateiras. Master thesis. University of Porto; 2016

[22] Silva A. A Litoestratigrafia e Estrutura do Supergrupo Dúrico – Beirão (Complexo Xisto-Grauváquico), em Portugal, e a sua correlação com as correspondentes sucessões em Espanha. Instituto Nacional de Engenharia, Tenologias e Inovação; 2005. pp. 2-26

[23] Silva PJABA. Mineralogia, Petrologia e geoquímica de Granitos e filões Aplito-pegmatíticos Da região de Guarda – Sabugal. PhD thesis. University of Trás-os-Montes e Alto Douro; 2014

[24] Sousa MB, Lowell GR. "Skarns" (W-F) Da auréola Do maciço granítico de Tabuaço (NE Portugal). III Congresso Nacional de Geologia. Sociedade Geológica de Portugal. Coimbra. 1991

[25] Cerejo T, Santos JF, Sousa JC, Castanho N, Sérgio G, Ribeiro S. Geochronology and isotope geochemistry of granitoids and metasediments of São Pedro das Águias area (Tabuaço W project). Comunicações Geológicas, 101. Especial I. 2014:61-64

[26] Ferreira N, Macedo CR, Sousa MB. Cronostratigrafia dos granitos da região de moimenta da beira – Tabuaço – Penedono. Memórias do Museu Laboratório Mineralógico e Geológico da Universidade do Porto, 1. 1987. pp. 287-301

[27] António T, Cerejo R. Geoquímica Da área de São Pedro Das Águias – Concessão de Tabuaço. University of Aveiro; 2013. Master thesis

[28] Dawson KM. Skarn Tungsten. Geology of Canadian Mineral Deposit Types, Geological Survey of Canada, Geology of Canada, No. 8. 1996. pp. 495-502

[29] Einaudi MT, Meinert LD, Newberry RJ. Skarn deposits: Economic Geology 75th Anniversary Volume. 1981:317-391

[30] Kwak TAP. W-Sn Skarn deposits and related metamorphic Skarns and Granitoids. Developments in Economic Geology. 1987;**24**:1-451

[31] Sato K. Characteristics of tungsten skarns in Japan, two contrasting types. Symposium on Tungsten Geology Jiangxi, China. 1982:203-210

[32] Sánchez SMT, Benito MCM, Pérez MLC. Mineralogical and physiochemical evolution of the Los Santos Scheelite skarn, Salamanca, NW Spain. Economic Geology. 2009;**104**:961-995

[33] Wesolowski D. Geochemistry of Tungsten in Scheelite Deposits: The Skarn Ores at King Island, Tasmania. Ph.D. Thesis. Pennsylvania State University; 1984

[34] Newberry RJ. W- and Sn-skarn deposits: A 1998 status report: Mineralogical Association of Canada Short Course Series. 1998;**26**:289-335

[35] Meinert LD, Dipple GM, Nicolescu S. World Skarn deposits. Economic Geology 100th Anniversary Volume. 2005:299-336

[36] Korzhinskii DS. Theory of Metasomatic Zoning (Trans. Jean Argrell). New York, Oxford: Clarendon Press; 1970. p. 162

[37] Newberry RJ, Einaudi MT. Tectonic and geochemical setting of Tectonic and Ore Deposits. Tucson, Ariz. March 19-20, Proc, 1981

[38] Meinert LD. Application of Skarn deposit zonation models to mineral exploration. Exploration and Mining Geology. 1998;**6**(2):185-208

[39] Mathieson GA, Clark AH. The Cantung E-zone scheelite skarn ore body, N.W.T.: A revised genetic model. Economic Geology. 1984;**79**(5):883-901

[40] Bird DK, Schiffman P, Elders WA, Williams AE, McDowell SD. Calc-silicate mineralization in active geothermal systems. Economic Geology. 1984;**79**:671-695

[41] Frisch CJ, Helgeson HC. Metasomatic phase relations in dolomites of the Adamello alps. American Journal of Science. 1984;**284**:121-185

IntechOpen